MEMO

Project No.:	**5238-881971**
Date:	**11.04.2024**
From:	5.1.2.e [redacted]
To:	5.1.2.e [redacted]
Copy to:	**DEEP.KBB intern**

DEEP.KBB Subsidence Model

1 Structure of subsidence model

The DEEP.KBB subsidence model can be divided into two main parts including separate calibration and validation processes:

1. Calculation of cavern volumes to derive convergence volumes as input for the next part
2. Calculation of surface deformations

Within the analytical model, these parameters and processes are calculated independently at first. In a subsequent step, the results will be combined to calculate and validate the convergence volume.

2 Convergence Calculations

The general structure of the first part of the model is depicted in Figure 2-1.

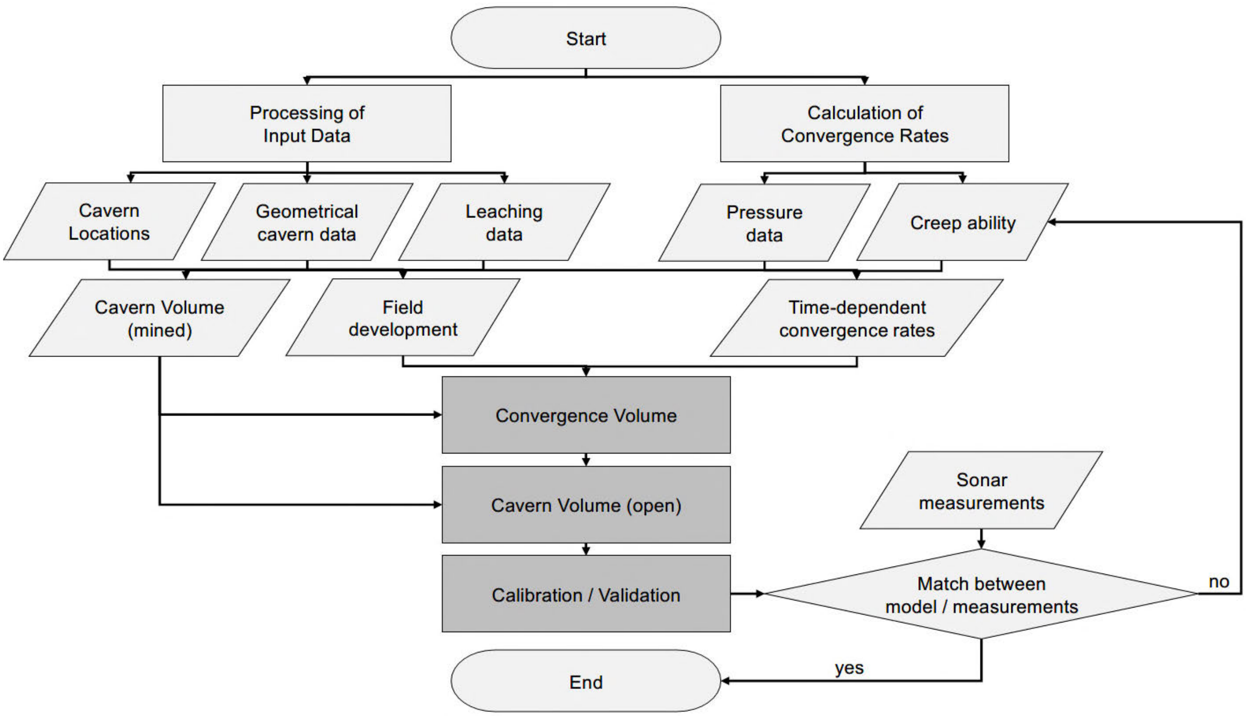

Figure 2-1: Structure of the Subsidence Model (Part 1 – Calculation of Convergence Volumes)

For the prediction of surface subsidence, a sophisticated understanding of the processes in the subsurface has to be established. As an input parameter for the subsidence calculations, the development of cavern convergence over time is of particular interest.

Therefore, a reliable determination of the in-situ creep ability of the host-rock material has to be carried out.

In general, the following processes are included in the confidence building of the subsurface processes:

1. Increasing cavern volume due to brine production considering a varying cavern depth over time
2. On-going cavern convergence
3. Increase of cavern convergence with increasing depth and cavern volume as well as lower internal cavern pressure
4. Verification of the volume development over time by comparison and correction of calculated cavern development with sonar measurements

The creep ability of rock salt is dependent on the effective stress, temperature and microstructural salt properties. The creep ability can be derived from lab tests as a first indication. However, since lab tests are conducted on cores from a specific location and depth region, cores are not always representative for the whole cavern area and some effects measured in the laboratory cannot be easily scaled up to a cavern-scale, the average in-situ creep behaviour of the salt rock mass surrounding a cavern can be derived more reliably from a history matching of the actual volume development during the operational life time (brine production/gas operation) of a cavern. In the history matching process, the observable volume of a cavern will be calculated and compared to the results of regularly conducted sonar measurements. The observable volume describes the volume of a cavern that can be captured by a sonar measurement.

Main calculated parameters in the first step are:

- the mined cavern volume representing the volume that has been mined by leaching,
- the sump volume representing the volume of insolubles that accumulated at the cavern bottom during the leaching process,
- the open cavern volume representing the cavern volume that is not filled with insolubles and can be detected via sonar measurements,
- the field development and
- the time-dependent convergence rates

2.1 Calculation of mined Cavern Volume

For the calculation of cavern volumes over time, leaching data are implemented into the model. Based on the produced brine volumes as well as the saturation of the brine, the mass of salt extracted from the subsurface is determined per cavern. Afterwards the mined cavern volume can be derived taking into account the pure salt density as well as the insoluble content.

Input:

- Brine production rates in m^3
- Equivalent concentration of Cl- in brine in eq/l
- Insoluble content in Vol-%
- Pure salt density in t/m^3

Output:

- Mined cavern volume in m^3

2.2 Determination of the Field Development

In this context, the field development includes all geometrical and spatial data as well as the timeframes for the different life cycle phases of the caverns. All geometrical and spatial data are independent from each other, so that for example maximum diameters can be set for calculations without changing cavern volumes. Generally, this analytical model is a 1D-approach considering depth, pressure and temperature data for individual caverns and spatial relations between different caverns and geological layers, i.e. the salt dome boundaries, via (azimuthal) distances.

In the following, input parameters to cover the field development are listed.

Well Locations:

- Coordinates of the wellhead
- Coordinates of the Last Cemented Casing Shoe (LCCS)
- Depth of the LCCS in m TVD
- Final drilling depth in m TVD

Geology:

- Depth of top of salt in m TVD
- Salt dome boundaries in different depths
- Density overburden in t/m³
- Density salt in t/m³
- Surface temperature in °C
- Temperature gradient overburden in K/m
- Temperature gradient salt in K/m

Timeframes for cavern development:

- Start and end of leaching
- Start and end of storage operations
- Start and end of the waiting period to reach thermal equilibrium
- Start and end of the technical abandonment phase
- Start and end of the post-mining phase, whereby the time period is defined by the client and can theoretically last until the caverns are totally converged

Cavern geometry over time (step-wise):

- Depth start leaching in m TVD
- Depth cavern sump in m TVD
- Depth cavern roof in m TVD
- Depth of centre of the cavern volume in m TVD
- Cavern volume (open or detectable via sonar measurements)
- Maximum cavern diameter in m
    - If the maximum cavern diameter is given, the centre of gravity is assumed at the same coordinates as the LCCS

– Alternatively, the maximum radius of the cavern envelope with a distance and azimuthal inclination from the centre of gravity of the existing cavern envelope and the coordinates of the LCCS can be used

These input parameter serve as a basis for convergence calculations. Furthermore, pillar dimensions between caverns are derived.

2.3 Time-dependent convergence rates

Creep response is calculated using an analytical formula as given by [VAN SAMBEEK 1993]. This formula (see Equation 1) represents the long-term creep response of a cylindrical cavern based on the material law of NORTON-HOFF.

$$\frac{\dot{V}}{V} = -\sqrt{3} \cdot \left[\frac{\sqrt{3}}{n} \cdot (P_\infty - P_i) \right]^n \cdot A \cdot e^{\left(-\frac{Q}{R \cdot T}\right)}$$

Equation 1

with:

$\dot{V}$	volumetric change rate (m³/d)
V	cavern volume (m³)
P_∞	geostatic pressure (MPa)
P_i	internal cavern pressure (MPa)
n	stress exponent (-)
A	structural parameter (1/(d * MPa^n))
Q	activation energy (kJ/mol)
R	gas constant (kJ/mol/K)
T	rock mass temperature (K)

To account for linear and non-linear creep, for convergence calculations the NORTON-HOFF power law has been applied with two branches (BGRc):

$$\dot{\varepsilon}_{eff} = A_1 \cdot \exp\left(-\frac{Q_1}{R \cdot T}\right) \cdot \left(\frac{\sigma_{eq}}{\sigma^*}\right)^{n_1} + A_2 \cdot \exp\left(-\frac{Q_2}{R \cdot T}\right) \cdot \left(\frac{\sigma_{eq}}{\sigma^*}\right)^{n_2}$$

Equation 2

with:

$\dot{\varepsilon}_{eff}$	creep rate (1/d)
A_1 / A_2	structural parameter (1/(d * MPa^n))
Q_1 / Q_2	activation energy (kJ/mol)
n_1 / n_2	stress exponent (-)
A	structural parameter (1/(d * MPa^n))
Q	activation energy (kJ/mol)
R	gas constant (kJ/mol/K)
T	rock mass temperature (K)
σ_{eq}	effective von Mises stress (MPa)
σ^*	stress scaling factor = 1 MPa

Through the choice of different structure parameters A_1 and A_2, activation energies Q_1 and Q_2 as well as stress exponents n_1 and n_2, it allows to consider different deformation mechanisms in dependency of the effective von Mises stress σ_{eq} and the Temperature T.

Salt creep at low deviatoric stresses has been inter alia recently investigated by [ECOLE POLYTECHNIQUE ET AL. 2020]. Therein, based on long-term lab-tests as well as long-term tests in the Altaussee Mine in Austria, in a range of low equivalent stress (0.2 to 5 MPa), the pressure solution creep mechanism could be identified as the main creep mechanism [URAI & SPIERS 2007]. The onset of pressure solution creep is expected to be dependent on the temperature and also the grain size of salt [URAI, SCHMATZ & KLAVER 2019].

The stress exponent of this creep mechanism is defined with n = 1. In the lower stress region, the stress exponent n was for example experimentally back-calculated by [GÜNTHER ET AL . 2016]. For “clean” salt n was determined to be 2, while for argillaceous salt n was determined to be 1. It should be noted that a detailed microstructural analysis on the tested cores has not been performed in mentioned literature.

In the higher differential stress range, dislocation creep is the predominant mechanism. For dislocation creep, generally stress exponents n between 3 and 5 are chosen based on results from the laboratory.

Since creep-properties are always specific for the location, they have to be determined by creep tests or by monitoring the long-term behaviour of the subsurface volume of a cavern to gain reliable values for the parameter of Equation 2. An exemplary creep characteristic based on lab tests is depicted in Figure 2-2.

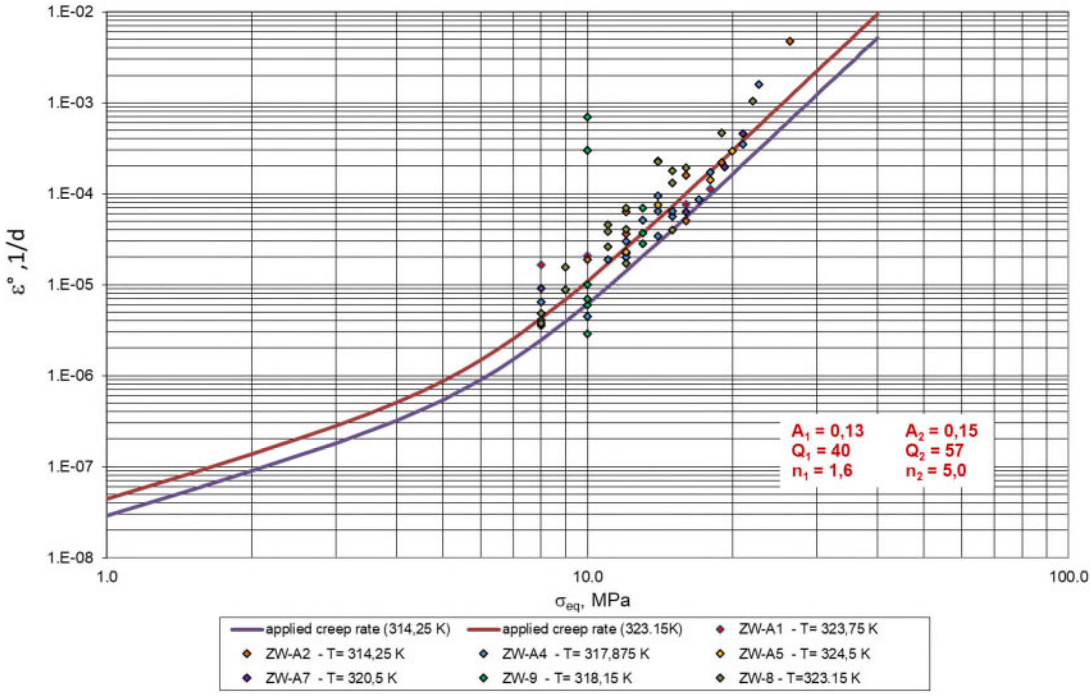

Figure 2-2: Creep characteristics derived from lab test results in high deviatoric stress range [LANGER, 1991], [BRÜCKNER, 2009], [BRÜCKNER, 2012]

With regard to tall cylindrical caverns, the stress profile as well as the temperature profile with depth is taken into account. For the reference depth for subsidence and convergence calculations, different alternatives are possible to use in a subsidence model. [SCHOBER ET AL. 1987] recommended the reference point to be calculated according to Equation 3 for subsidence calculations.

$$T_{RD} = \sqrt{z_{sump} \cdot z_{roof}}$$

Equation 3

with:
- z_{sump} depth of the cavern sump (m TVD)
- z_{roof} depth of the cavern roof (m TVD)
- T_{RD} reference depth (m TVD)

With respect to caverns of varying partial volumes with depth different depth ranges can be specified, as this is done for the calculation of the convergence in the studies of [EIKEMEIER & HEUSERMANN, 2007].

The reference depth for subsidence modelling as well as for convergence modelling can also be assumed by the depth of centre of the cavern volume, which is determined from the sonar measurements. Thereby the representative depth can change over time. This represents the leaching process that starts from the bottom and volume increase is developed upwards.

The BGRc-model is considering only steady-state creep and is used within the DEEP.KBB subsidence model because its simplicity is suited especially for analytical subsidence prediction models, since the impacts of transient creep or high temperature deviations are very difficult to validate in those models [BEREST AND BROUARD 1998], while still sufficient results will be achieved if an adequate calibration and validation of the creep ability is executed.

In the history matching process, for convergence calculations Equation 1 with two branches (see [WEP 2010]; [WEP 2015]), to account for pressure solution and dislocation creep, has been proven as effective. This does represent an approximate solution for the calculation of the convergence under consideration of two creep mechanisms, since it does not explicitly determine at which distances from the cavern wall pressure solution or dislocation creep is dominant.

Therefore, for the prognosis an adapted model according to Equation 4 is utilized [BEREST ET AL, 2008], [VAN SAMBEEK & DIRIENZO 2016].

$$\frac{\dot{V}}{V} = -\sqrt{3} \cdot \left[\frac{\sqrt{3}}{n_2} \cdot (P_\infty - P_i)\right]^{n_2} \cdot A_2 \cdot e^{\left(-\frac{Q_2}{R_m \cdot T}\right)} \cdot \left[1 + \frac{(n_2 - n_1)S}{\sqrt{3}(P_\infty - P_i)}\right]^{n_2}$$

Equation 4

with:

S	Transition from pressure solution creep to dislocation creep (MPa)
A_2	structural parameter dislocation creep (1/(d * MPa^n))
Q_2	activation energy dislocation creep (kJ/mol)
n_2	stress exponent dislocation creep (-)
n_1	stress exponent pressure solution creep (-)

Within the equation, the convergence resulting from dislocation creep is multiplied by a factor which is dependent on the magnitude of the pressure solution creep. The magnitude is defined by the stress exponent n_2 as well as the parameter S, which is the stress level at which the transition between pressure solution dominant and dislocation dominant creep occurs. Equation 4 separates the rock mass surrounding the cavern in two parts, so that in dependence of the difference between P_∞ and P_i a stress distribution is calculated, in which pressure solution creep is dominant when σ_{eq} < S and dislocation creep is dominant when σ_{eq} > S.

Therefore, S represents in a creep curve the intersection point between the pressure solution and the dislocation creep. To sufficiently account the pressure solution creep characteristic, also Equation 2 was extended by a temperature and grain size dependency for the pressure solution creep according to [URAI & SPIERS 2007]:

$$\dot{\varepsilon}_{eff} = \frac{b}{TD^3} \cdot \exp\left(-\frac{Q_1}{R \cdot T}\right) \cdot \left(\frac{\sigma_{eq}}{\sigma^*}\right)^{n_1} + A_2 \cdot exp\left(-\frac{Q_2}{R_m \cdot T}\right) \cdot \left(\frac{\sigma_{eq}}{\sigma^*}\right)^{n_2}$$

Equation 5

with:

b	structural parameter (1/(d * MPa^n)
D	grain size (m)

Input data for these calculations are:

- Geological data and cavern geometries as listed in section 2.2.
- Time-dependent medium within the cavern as per timeframes for cavern development in section 2.2
- Daily wellhead pressures

As a result, pressure-dependent convergence rates are calculated within this step.

2.4 Prediction of Convergence Volumes

In general, it is considered that the cavern sump, where insoluble content has settled, represents an active volume regarding cavern convergence, meaning that the volume for convergence calculations consists of the open cavern volume, the volume of insolubles in the cavern sump as well as the pore volume in the cavern sump. To calculate the time-dependent convergence volume of a cavern, it is considered that whole mined cavern volume (open cavern volume + cavern sump volume) is actively contributing to cavern convergence. In the calculation, bulk density and possible strength of the sump material is excluded, which is a conservative assumption.

For a single time-step, the previously accumulated mined cavern volume minus the previously accumulated convergence volume, the mined cavern volume within the time step, the pressure at reference depth, the pressure dependent convergence rate and an empirical factor to account for the salt pillars between the caverns are considered:

$$V_{conv}(\Delta t) = \left(V_{mined}(t - \Delta t) - V_{conv}(t - \Delta t) + \frac{V_{mined}(\Delta t)}{2}\right) \cdot \dot{V}(p) \cdot \dot{K}$$

Equation 6

with:	Δt	time step (d)
	p	pressure at reference depth (bar)
	V_{conv}	convergence volume (m^3)
	V_{mined}	mined cavern volume (m^3)
	$\dot{V}$	volumetric change rate (m^3/d)
	$\dot{K}$	correction factor based on salt pillars to neighbouring caverns (-)

The correction factor $\dot{K}$ is based on the observation that for a single cavern in a salt deposit the creep response is smaller than for the same cavern located in the middle of a field of several neighbouring caverns. This effect is considered according to Equation 4 based on field observations [ZANDER 2007].

$$\dot{K} = 2.6 \cdot \left(\frac{pillar}{diameter}\right)^{\left(-\frac{1}{0.6}\right)} + 1.28$$

Equation 7

with:	pillar	average salt pillar to cavern neighbours (m)
	diameter	maximum cavern diameter (m)

2.5 Calculation of open cavern volume

The observable or open cavern volume can be determined using following equation:

$$V_{\mathrm{obs}} = V_{\mathrm{mined}} - V_{\mathrm{conv}} - V_{\mathrm{sump}}$$

Equation 8

with:	V_{obs}	open cavern volume
	V_{mined}	mined cavern volume
	V_{conv}	convergence volume
	V_{sump}	sump volume

The mined cavern volume V_{mined} can be determined based on the mass of produced salt and the volume of insolubles that accumulate with a certain bulking factor at the cavern sump, resulting in V_{sump}. This bulking factor can be specified for every cavern individually.

The calculated open cavern volume represents a validation value for the model, because it can be compared to sonar measurements during the operation of a cavern to determine differences within modelled and real data.

2.6 Calibration/Validation

The calibration and validation process is utilized to determine the optimal set of parameters to determine the convergence volume as an input parameter for the subsidence prediction.

Main model parameters in this regard are the different structure parameters A_1 and A_2, activation energies Q_1 and Q_2 as well as stress exponents n_1 and n_2. In the first model run, these parameters are derived based on lab tests results for the creep behaviour of the salt at the specific location. If lab data are not available, parameters can also be assumed based on experience from comparable locations.

After the run of the first part of the model, the calculated open cavern volumes are compared to sonar measurements.

An example of the validation process is depicted in Figure 2-3. The dark blue line depicts the modelled cavern volume over time, the light blue line shows the convergence volume over time, while the green squares depict cavern volumes determined by sonar measurements.

Based on the difference between measured and calculated volumes, the parameters A_1 and A_2, Q_1 and Q_2 as well as the stress exponents n_1 and n_2 will be adapted from the original creep characteristic until a sufficient fit is achieved. Thereby, the general creep characteristics, e.g. the deformation mechanisms n_1 and n_2 and the activation energy Q_1 and Q_2, should stay the same as derived from lab tests.

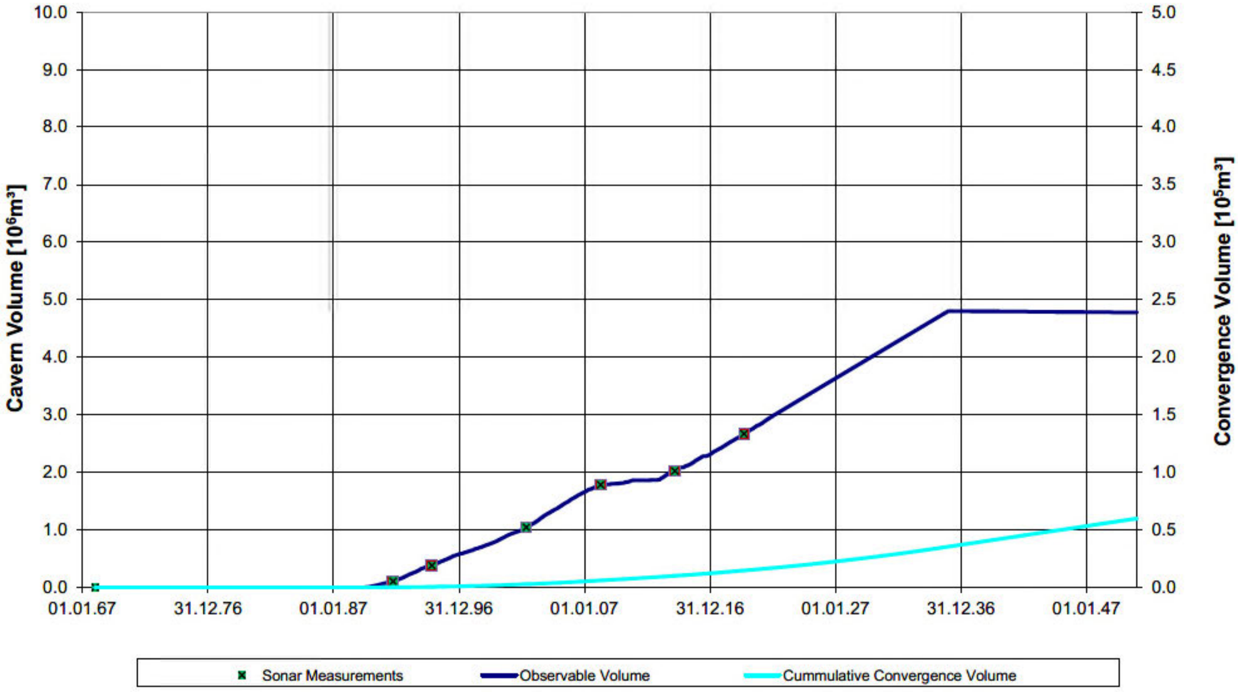

Figure 2-3: Schematic illustration of the calibration/validation process for convergence

2.7 Discussion of Uncertainties

Based on the volume development due to the mined cavern volume and the sump volume, the in-situ creep ability of the rock mass can be fitted to the sonar measurements.

However, since a model represents a simplification of the reality, a certain level of inaccuracies is implied in the calculation of the volume development.

The main inaccuracies for the calculated cavern development can be derived from the following sources:

- Produced brine volume
- Salt concentration in brine
- Insoluble content of the salt
- Pressure-dependent generation of convergence volume
- Geological interpretation
- Microstructural influences

Furthermore, the validation values (sonar measurements) imply inaccuracies as well. With regard to the measured cavern volume, generally a measurement error of up to 1 % occurs. If measured through one pipe, for example a leaching string, the measurement error can generally be expected in the range of 2-4 %. Furthermore, in the case of irregularities in the cavern wall like backpockets, not all parts of the cavern might be detected by sonar measurement. Therefore, the volumetric error of sonar measurements can additionally increase. This error might reach values above 5 % of the total cavern volume for caverns with a highly irregular form. This has to be taken into account when using the sonar measurements for validation of the volume development. Therefore, the volumes given by sonar measurements need to be interpreted in case backpockets are identified.

In the course of the validation process, the aim is to achieve that the cumulated difference between the measured and the calculated subsidence values is in the range of or below 20% in relation to the calculated convergence volume. In comparison thereto, the deviation between calculated and measured volume would be significantly lower. By assigning the complete deviation between modelled and measured cavern volume to the convergence volume, all relevant above-mentioned inaccuracies are assigned to the convergence volume.

As a conservative approach, for future convergence calculations, a creep ability determined by the Cavern Closure Consortium (CCC) based on creep tests and microstructural investigations is considered in comparison to the creep ability derived from the history matching process. This bayesian approach utilizes data from lab-scale (creep tests/mine tests) which also considers impurity content and grain size of each sample. The approach is then verified against creep derived from pressure build-up curves and modelling efforts on the dome-scale.

To account for uncertainties within the determination of the creep ability, an expected creep ability, utilizing a mean grain size of the salt formation in Equation 5, as well as a conservative creep ability, utilizing a lower grain size in Equation 5 and thereby increasing the influence of the pressure solution creep, is used for convergence calculations.

3 Calculation of Surface Deformations

The general structure of the second part of the model is depicted in Figure 3-1.

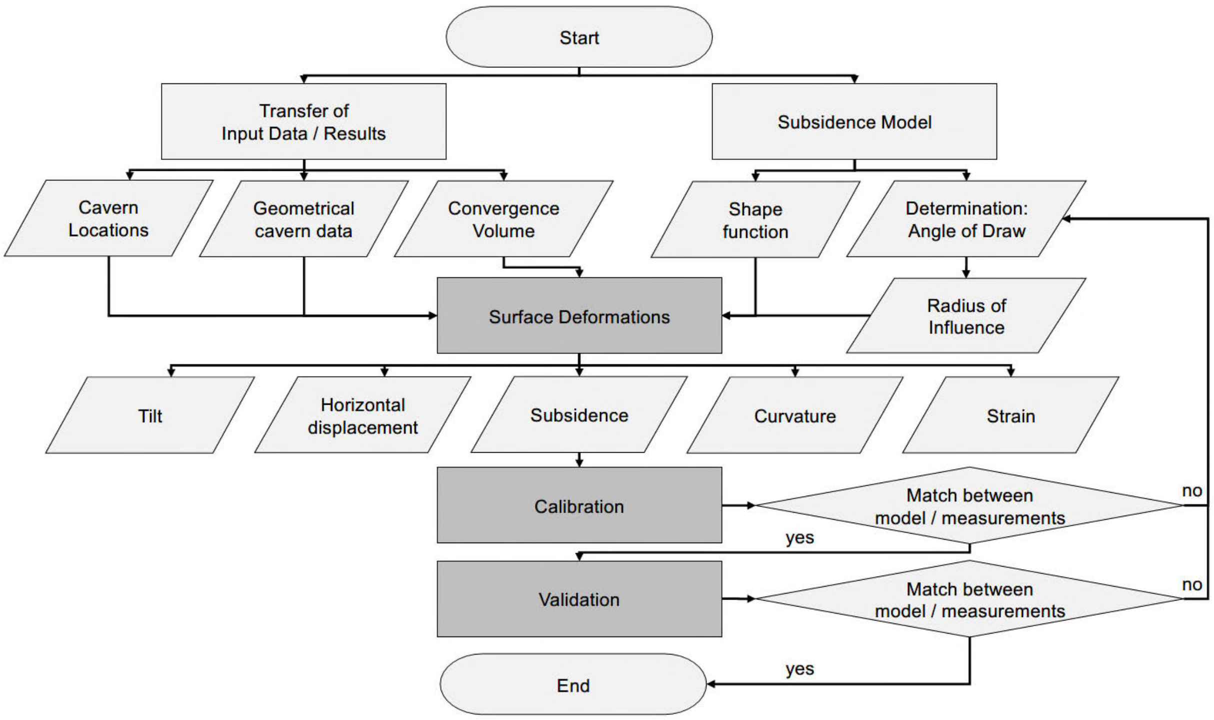

Figure 3-1: Structure of the Subsidence Model (Part 2 – Calculation of Surface Deformations)

For the calculation of surface deformations, the same geometrical and spatial parameters are applied as for the calculations of convergence volume in part 1 of the subsidence model. Furthermore, the time-dependent convergence volume determined in the previous steps for the individual caverns is used as an input parameter.

3.1 Shape function

In order to describe the transfer of the convergence volume to the surface, an influence shape function is utilized. Based on the calculated convergence volume V_{conv}, the subsidence prediction is carried out by using an extended analytical approach of [SROKA & SCHOBER 1982]. This approach uses a gaussian function defined by a radius of influence to describe the subsidence bowl. It is based on the principle of rotational symmetry. The rock mass structure surrounding the cavern is assumed to be isotropic. In reality, however, anisotropies occur due to the salt dome geometry, different rock layers and faults above caverns.

Therefore, the calculation formula of [SROKA & SCHOBER 1982], that generates a circular subsidence bowl on the surface above a cavern, was extended through the introduction of the azimuth φ [QUASNITZA 1988]. The azimuth is defined as the horizontal angle between the cavern axis and the point, where the subsidence is calculated. The applied modification of the calculation formula of [SROKA & SCHOBER 1982] is shown in Equation 9 according to [BUZOGANY 2019] by describing the horizontal shape of the subsidence bowl through a defined number n_{rad} of radii of influence (see Figure 3-2). For the optimization of computational times in combination with sufficient results, the number of radii of influence is generally chosen to be n_{rad} = 8.

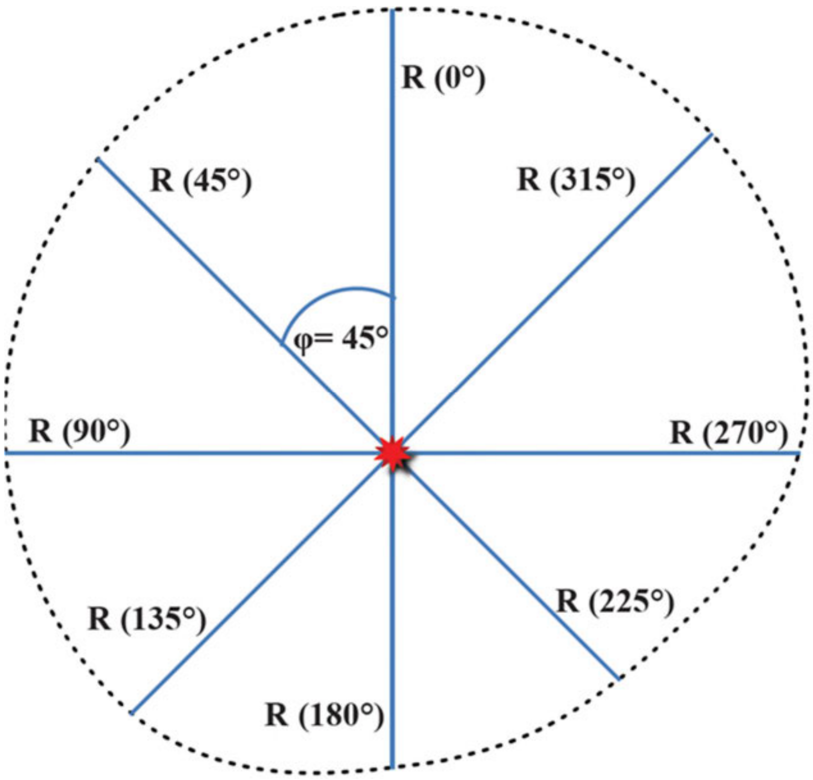

Figure 3-2: Schematic representation of the subsidence bowl defined by eight radii of influence

$$s(r,t,\varphi) = a(t) \cdot V_{\mathrm{conv}}(t) \cdot \frac{1}{(\frac{1}{n}\sum_{i=1}^{n} R(\varphi = i \cdot (\frac{360}{n})))^2} \cdot \exp(-\pi \left(\frac{r}{R(\varphi)}\right)^2)$$

Equation 9

with:
- s subsidence (m)
- a transmission factor (-)
- V_{conv} convergence volume (m³)
- $R(\varphi)$ radius of influence in dependence of the azimuth (m)
- r horizontal distance cavern centre – calculation point (m)

Accordingly, the maximum subsidence above the centre of a cavern (horizontal distance cavern centre – calculation point r = 0) for a specified point in time t is calculated by considering the average radius of influence R of the total subsidence bowl. The values for $R(\varphi)$ in between a defined number of n sectors are calculated using an elliptical interpolation function. The transmission factor a is conservatively considered to be 1 in this equation. Therefore, all volume losses from the subsurface will be transmitted to the surface. If any information about geological layers or other influences are available that would hinder transmission, the transmission factor a may be lowered.

The variation of the radius of influence is dependent on the distance between the centre of the cavern and the salt dome boundaries. To differentiate the transmission behaviour between the salt dome and the surrounding non-salt rock mass the angle of draw, which represents the angle between the reference point of the cavity and the most distant point of subsidence on the surface, is subdivided into an angle of draw for the salt dome β_s and an angle of draw for the surrounding non-salt rock mass β_N (see Figure 3-3).

As depicted in Figure 3-3, it is generally assumed that the angle of draw of the surrounding non-salt rock mass β_N would be greater than that of the salt rock [QUASNITZA 1988]. This can be related to the influence of the higher stiffness and lower strength of rock salt in comparison to many other geological layers. However, this has to be checked against observations. Therefore, the angle of draw for the non-salt rock mass β_N as well as the angle of draw for the salt dome are fitted as modelling parameters to the measured subsidence values to represent the local specific transmission behaviour of the overburden.

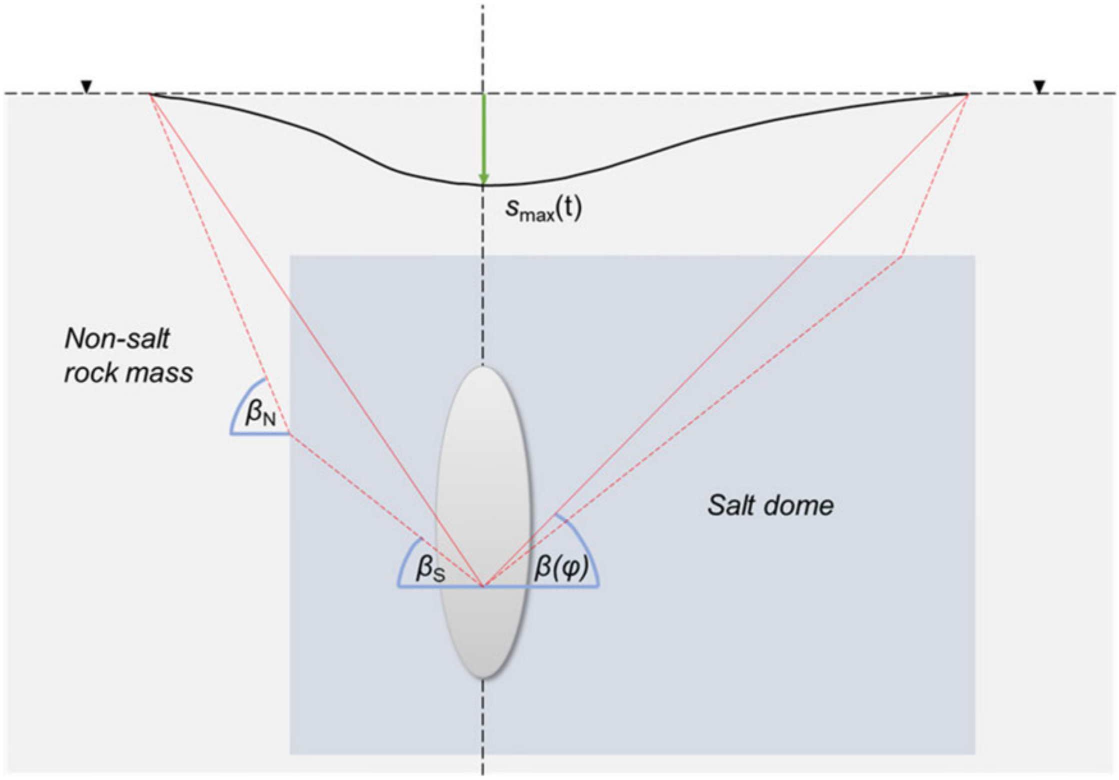

Figure 3-3: Differentiation of the angle of draw (salt dome and surrounding overburden)

The radius of influence versus depth is expressed by an exponential function. The intersection points between the angle of draw and the salt dome boundaries have to be calculated to evaluate the impact of the surrounding non-salt rock mass.

The distance, which is necessary to ensure that the subsidence of a cavern is not influenced by the salt dome boundaries, is calculated by determining the radius of influence of the caverns in different depths z. The equation is given by [SROKA ET AL. 2017]:

$$R(z) = R(0) \cdot \left[\frac{(z_{cav} - z) + c}{z_{cav} + c}\right]^{n_{int}}$$

Equation 10

The parameters c and n_{int} represent the cavern roof coefficient, which is dependent on the stiffness of the layer above the cavity, and the interface coefficient, respectively.

Recommended values for n lie between 0.45 and 0.70 [DŻEGNIUK, NIEDOJADŁO & SROKA 2003]. For n a value of 0.5 and for c a value of 1 m was chosen. The value of c = 1 m was chosen based on a calibration of the model for a cavern field with the value n = 0.5, in which surface subsidence and subsidence at the casing shoe of a cavern were measured over several decades. Since no subsidence below the surface is measured in the cavern fields Heiligerlee and Zuidwending, these values cannot be fitted with measurement results and represent approximations to calculate the function of the angle of draw inside the salt dome.

The calculation of the azimuthal angle of draw $\beta(\varphi)$ is realized by the interpolation between the angle of draw for the salt dome β_s and the angle of draw for the surrounding non-salt rock β_N. As interpolation value the ratio of the height fraction of the function of the angle of draw inside of the surrounding non-salt rock mass Δz_N to the total height of the overlying salt $\Delta z_{S,tot}$ is used.

$$\beta(\varphi) = \beta_S + (\beta_N - \beta_S) \cdot \frac{\Delta z_N}{\Delta Z_{S,tot}}$$

Equation 11

With the aim of a better illustration the components of Equation 11 are displayed in Figure 3-4.

Based on this procedure, subsidence will be calculated for every cavern individually. The final subsidence bowl results based on the principle of superposition, meaning individual subsidence shares will be superimposed over each other. This represents a simplification of the reality, because the directional deformations caused by a single cavern may be influenced by the deformations caused by neighbouring caverns. However, this approach has been proven as reliable for subsidence predictions above cavern fields (e.g. [SROKA ET AL. 1987], [HENGST 2014]).

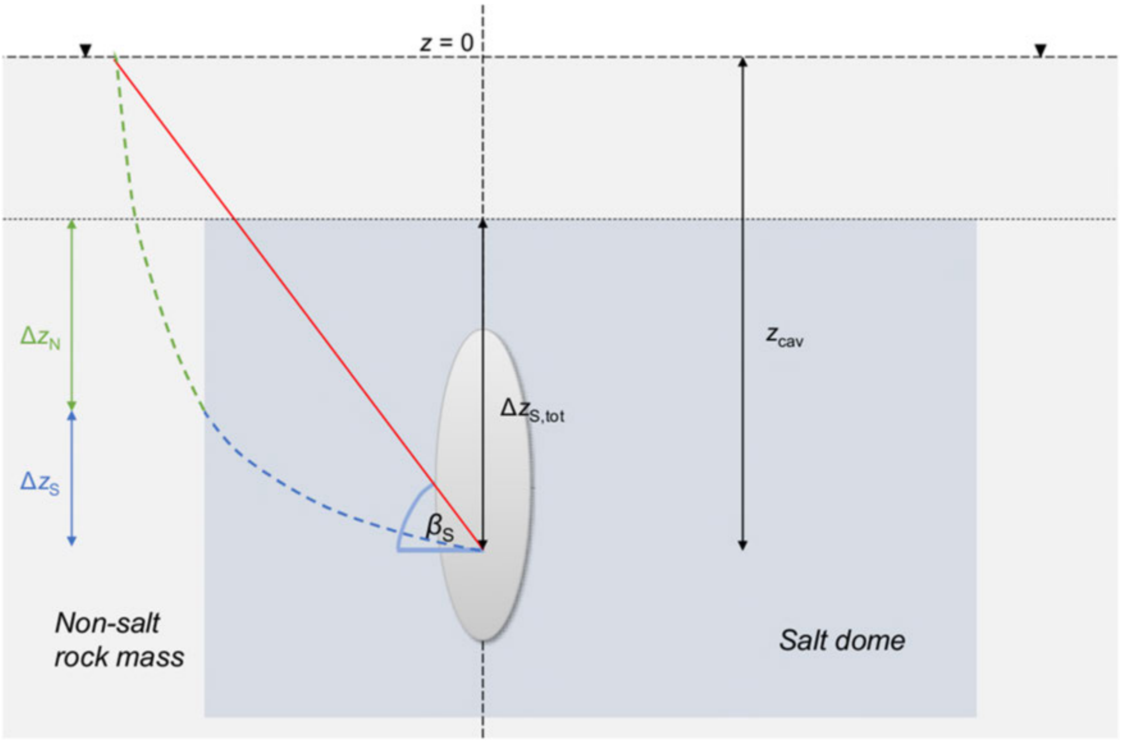

Figure 3-4: Schematic representation of the components of equation 11

3.2 Calibration/Validation of the Angle of Draw

The azimuthal angle of draw $\beta(\varphi)$ defines the azimuthal radius of influence $R(\varphi)$ and is dependent on the model parameters β_S and β_N. These parameters are calibrated and validated until a sufficient fit between modelled and measured subsidence values is achieved.

In the calibration/validation process, it has to be considered that different sources might contribute to the overall subsidence. These include for example:

- Subsidence due to cavern operations
- Subsidence due to processes in the shallow subsurface (e.g. soil compaction, water management)
- Subsidence due to other mining operations

The DEEP.KBB subsidence model only calculate subsidence due to cavern operations. Therefore, further information about subsidence due to other effects needs to be available to be considered. If no further information about other effects than subsidence due to cavern operations are available, the complete measured subsidence will be contributed to cavern operations. This can be seen as conservative, but subsidence shares due to cavern operations might be overestimated.

In the following, the calibration/validation process will be described in detail.

3.2.1 Validation of measured Subsidence at Benchmarks

In the first step, the measurement results itself were evaluated. In relation thereto, it should be stated that, in general, mining operation (gas production and cavern operation) will generate subsidence, while natural effects can cause either subsidence (e.g. due to ground compaction) or lifting (e.g. due to water management).

Since the natural effects are highly dependent on the surface conditions and the surface behaviour as well as on the specific conditions of the respective benchmark, it is not possible to define a value for the natural impact, which would be representative in general for the area investigated.

From a geomechanical point of view with regard to cavern operations, surface lifting cannot be explained (for cavern pressures below the lithostatic stress level, which is the case in the operational phase and during a soft shut-in, and without consideration of tectonics). Therefore, the benchmark points, which indicate lifting, are not suited to validate the subsidence model for cavern operations and will be neglected in the validation process.

If detailed information is not available, the measured subsidence values will not be corrected by natural effects. This can be seen as a conservative approach, since it is expected that natural effects would cause subsidence. Thus, by considering the observed subsidence as subsidence from cavern operations (and other mining operations, if applicable) will lead to a prediction of higher subsidence due to their operational impacts.

3.2.2 Calibration of the Angle of Draw

For the calibration of the angles of draw β_S and β_N, a set of representative levelling benchmarks is selected. These benchmarks should be equally distributed over the field of investigation and should also cover all relevant regions of the investigation area to calibrate the model parameters based on the maximum subsidence in the centre of the subsidence bowl as well as the shape of the subsidence bowl in different azimuthal directions. The limited number of benchmarks used for the calibration process enables to determine a simplistic approach to investigate the dependence of subsidence in different regions of the angle of draw.

In the first calibration run, β_S and β_N are set to be equal. This corresponds to the parameter β in the model of Sroka & Schober (1982). The average absolute difference between modelled and measured subsidence values is then compared for a reasonable number of calibration runs. The angle of draw β which achieves the lowest model error is then chosen as a basis for the following fine calibration. In the calibration process all reliable levelling campaigns at different points in time are considered.

Based on the value for β, β_S and β_N are varied to investigate if the calibration results can be improved. In this process, the maximum subsidence in the centre of the subsidence bowl can be kept the same as in the previous calibration step, while the shape of the subsidence bowl in different azimuthal directions can be varied. As in the step before, the average absolute difference between modelled and measured subsidence values is then compared for a reasonable number of calibration runs.

The best fit of β_S and β_N is then used for the validation of the model.

3.2.3 Validation of the angle of draw

Within the validation process, calculated and validated subsidence values are compared for all available benchmarks. The aim of the validation process is to prove that the calibrated angles of draw represent the whole measured subsidence bowl. Therefore, the fit between measured and calculated subsidence values for selected benchmarks from the calibration needs to be confirmed for all benchmarks.

To evaluate that the set of parameters represents the subsidence bowl, it has to be considered that the zero measurement for the benchmarks differs. Therefore, the absolute differences in between calculated and measured values would automatically be smaller for newer benchmarks.

In order to establish a common validation parameter, the calculated overall subsidence rate (mm/a) as well as the difference/error to the measured subsidence rate at the respective benchmark since the beginning of the measurement are calculated.

The benchmark points are then categorized according to the following principle:

very good	Difference between measurement and prediction up to 0.5 mm/a
good	Difference between measurement and prediction up to 1.0 mm/a
bad	Difference between measurement and prediction greater than 1.0 mm/a

On the one hand, this approach enables to evaluate the model accuracy without further interpretation of the results. In general, the validation should result in over 50 % of very good results and below 20 % of bad results to represent the subsidence bowl sufficiently.

On the other hand, a statistical approach on its own might not be able to explain all effects within the investigation area, especially if for example natural effects on subsidence have been neglected. Therefore, the categorization of the benchmarks should also be visualized as exemplary displayed in Figure 3-5. This enables to eliminate clear outliers. In Figure 3-5 for example, in the south of the cavern field one benchmark validation between several very good matches shows a bad match. In this case, a detailed investigation of the benchmark has to be carried out to identify whether the measurement result can be classified as an outlier or represents a model inaccuracy. Furthermore, in a distance of approx. 4 km to the west from the cavern field, several benchmarks indicate a bad match. These benchmarks are located mostly outside of the influence area of the subsidence bowl and in an urban area. The land use, infrastructure, soil sealing or the impact of other mining activities (in this region for example by NEDMAG) not considered in the subsidence model might impact subsidence in this area, meaning that benchmarks in this area might be not representative to evaluate subsidence due to cavern operations.

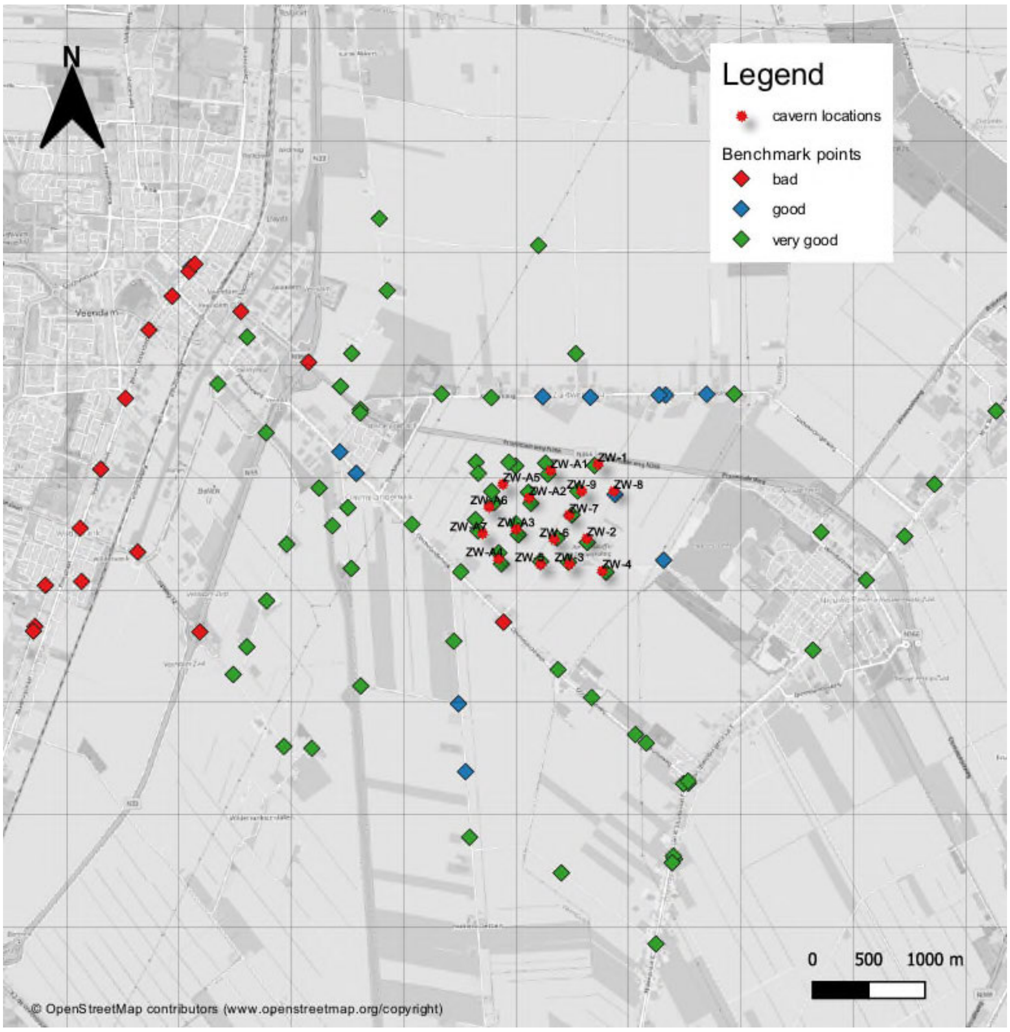

Figure 3-5: Validation of Subsidence Model on Benchmark Points

In contrast to the calibration process, the validation of the model so far only considers the latest levelling campaign by applying an average subsidence rate. To also include the development over time, subsidence is illustrated over time at all benchmarks.

This is exemplary depicted in Figure 3-6. In this case, subsidence due to cavern operations is superimposed by subsidence due to other mining activities. Measured subsidence values are depicted in red dots. Subsidence values due to other mining activities are depicted in orange dots. The light green line depicts the subsidence induced by gas storage caverns and the dark green line subsidence due to brine production caverns. The dark blue line depicts the subsidence due to all caverns since the start of the leaching of the first cavern in the field, while the grey line depicts the subsidence generated since the zero measurement of the respective benchmark. The yellow dots show the superposition of subsidence due to cavern operations and other mining activities. These values can be compared to the red dots and should approximately show an equal development over time. This part of the validation process serves as an additional verification of the statistically determined fit according to the evaluation criteria discussed beforehand and is only conducted visually.

All in all, the validation process is finished, when it has been shown that the utilized set of subsidence parameter for the subsidence model represents the measured subsidence bowl in a sufficient way, which is achieved by a statistical as well as a visual evaluation.

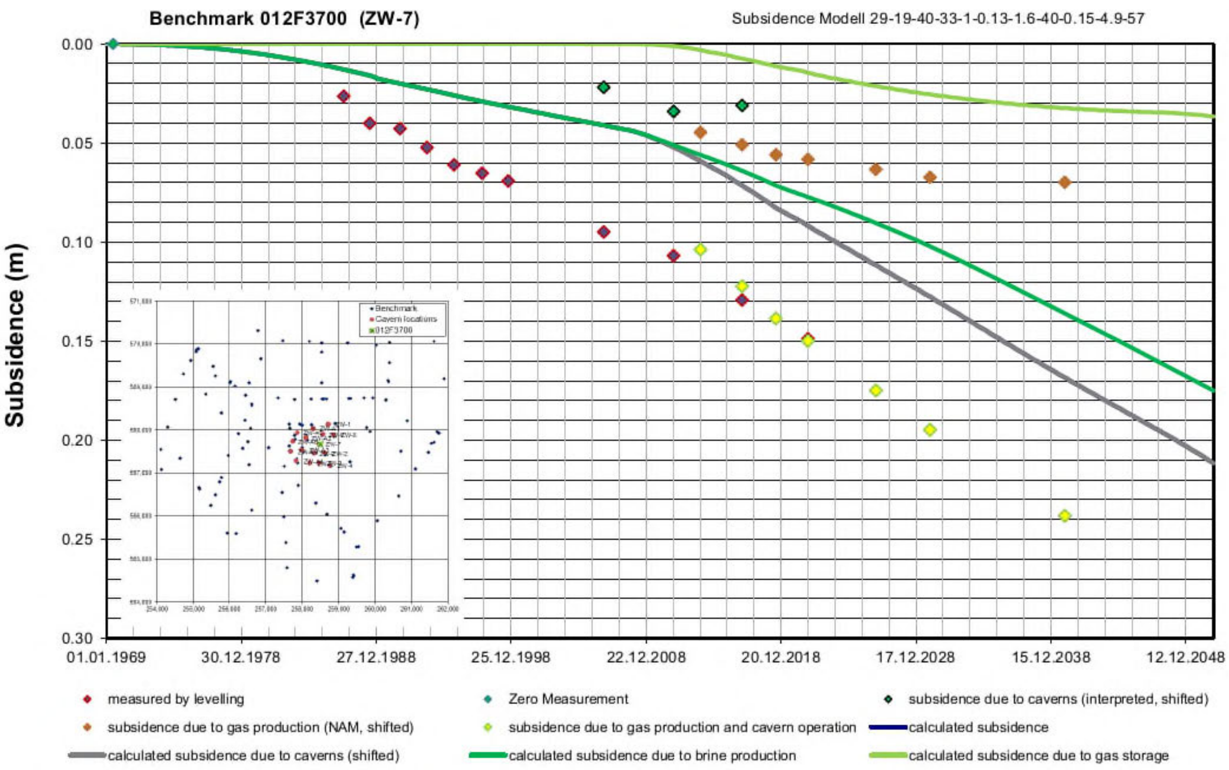

Figure 3-6: Development of subsidence over time at a levelling benchmark

3.3 Discussion of Uncertainties

In the process of subsidence modelling, different sources contribute as uncertainties and might result in inaccuracies of the model. These might originate from:

- Inaccuracies in the subsidence model
- Inaccuracies of levelling measurements

In general, every model represents a simplification of the reality. Therefore, differences within modelled and measured errors occur. That is why a history matching to validate the modelling approach and to evaluate the model accuracy is of high importance also to provide a sound model basis for future predictions. Within the history matching process, a sufficient fit between modelled and measured values can be achieved. However, even this fit implies that model and measurement do not perfectly match.

Furthermore, also levelling measurements involve certain accuracies. Tolerances for levelling measurements are generally dependent on the length of the levelling line. Standard deviations for a single levelling measurement can usually be expected to be in the range of 0 – 5 mm.

To account for these inaccuracies, a conservative approach for the subsidence model has been developed for the prediction of subsidence. This conservative approach mainly consists of two applied measures:

- The investigation of an expected and a conservative creep ability based on an investigation by the CCC.
- The contribution of subsidence due to natural effects and ground water production to subsidence due to cavern operations.

Since the subsidence model is fitted based on the calibrated/validated convergence volumes from part 1 of the subsidence model, the applied conservatism therein can also be directly transferred to part 2 of the subsidence model. The investigation of an expected and a conservative creep ability represents a range for the convergence results. Generally, the convergence based on these creep abilities is higher than within the history matching and the convergence resulting from the conservative creep ability represents an upper limit for resulting convergence based on microstructural investigations. The increase in creep ability ultimately results also in increased subsidence considering a specific point in time before total convergence, while the conservative approach also represent an upper limit for subsidence.

The second conservative assumption included in the model is that subsidence due to natural effects and due to water management are accounted towards subsidence due to cavern operations. In the Netherlands, subsidence due to natural effects is caused mainly by compaction, postglacial isostacy and tectonics [KOOI ET AL 1998]. For example, in the Wadden Sea, the natural subsidence is estimated to be in the range of up to 1 mm/a [FOKKER 2018].

For the Zuidwending/Heiligerlee cavern fields, natural subsidence rates of 0.33 mm/a have been assumed in the past [PÖTTGENS, 1973], while in Heiligerlee additionally subsidence due groundwater production until 1996 for cavern leaching contributed to the overall subsidence.

For example, when applying the rate of 0.33 mm/a to the timespan of 51 years since the first levelling measurement in the Zuidwending area, the influence of natural effects of subsidence would amount to approx. 17 mm. Related to the matched maximum subsidence of 93 mm, this amounts to approx. 18% and would cover inaccuracies due to levelling errors and is also in the range of uncertainties implied by convergence calculations. It has to be stated, that these values for natural subsidence rates have not been validated and shall only be used to show the potential influence on the results of the subsidence model by the neglection of subsidence due to natural effects.

4 Post-mining phase

4.1 Abandonment Scenario: Hard Shut-In

In the hard shut-in scenario, the cavern well will be plugged and cemented to completely seal of the brine filled cavern from the surface and also from the geological layers above the salt section. In this scenario, no further pressure control inside of the cavern is possible.

After the end of production, a waiting time is considered for each cavern before the cavern will be plugged in a brine-filled state in the hard shut-in scenario. The waiting time shall ensure that a temperature close to the thermal equilibrium is reached between the brine inside the cavern and the surrounding salt to reduce the pressure increase in the cavern due to brine heating during the shut-in phase.

Directly at shut-in, the cavern pressure equals the weight of the brine column up to the surface, which is lower than the stress gradient of the surrounding salt mass. In the following period the cavern pressure will increase mainly due to convergence, while thermal effects can be considered as negligible after the waiting period, and finally reach the lithostatic rock mass stress at the cavern roof. Shortly before reaching the lithostatic rock mass stress, the process of brine infiltration into the rock mass will start as a result of microcrack opening, beginning at the surface of the cavern roof or slightly below the plugging depth/last cemented casing shoe. This will introduce a secondary induced permeability in the salt, which was originally technically tight.

During the subsequent phase of abandonment, the brine infiltration, percolation or permeation process will continue and spread in the salt, as convergence will still take place in the lower part of the cavern, provoking an overall pressure increase, which will be equalized in the upper part of the cavern by brine migration. Laboratory experiments performed in different laboratories as well as in-situ tests have shown that the migration of brine already occurs when the fluid pressure is slightly below the minimum in-situ stress in the salt mass, i.e. the induced secondary permeability was high enough to balance the pressure increase (e.g. [BROUARD ET AL. 2001], [MINKLEY ET AL . 2013]). Therefore, the cavern pressure at the cavern roof can be considered to be slightly lower than the lithostatic pressure during hard shut-in (see Figure 4-1). In the model, this pressure is an assumed equilibrium pressure, which needs to be verified.

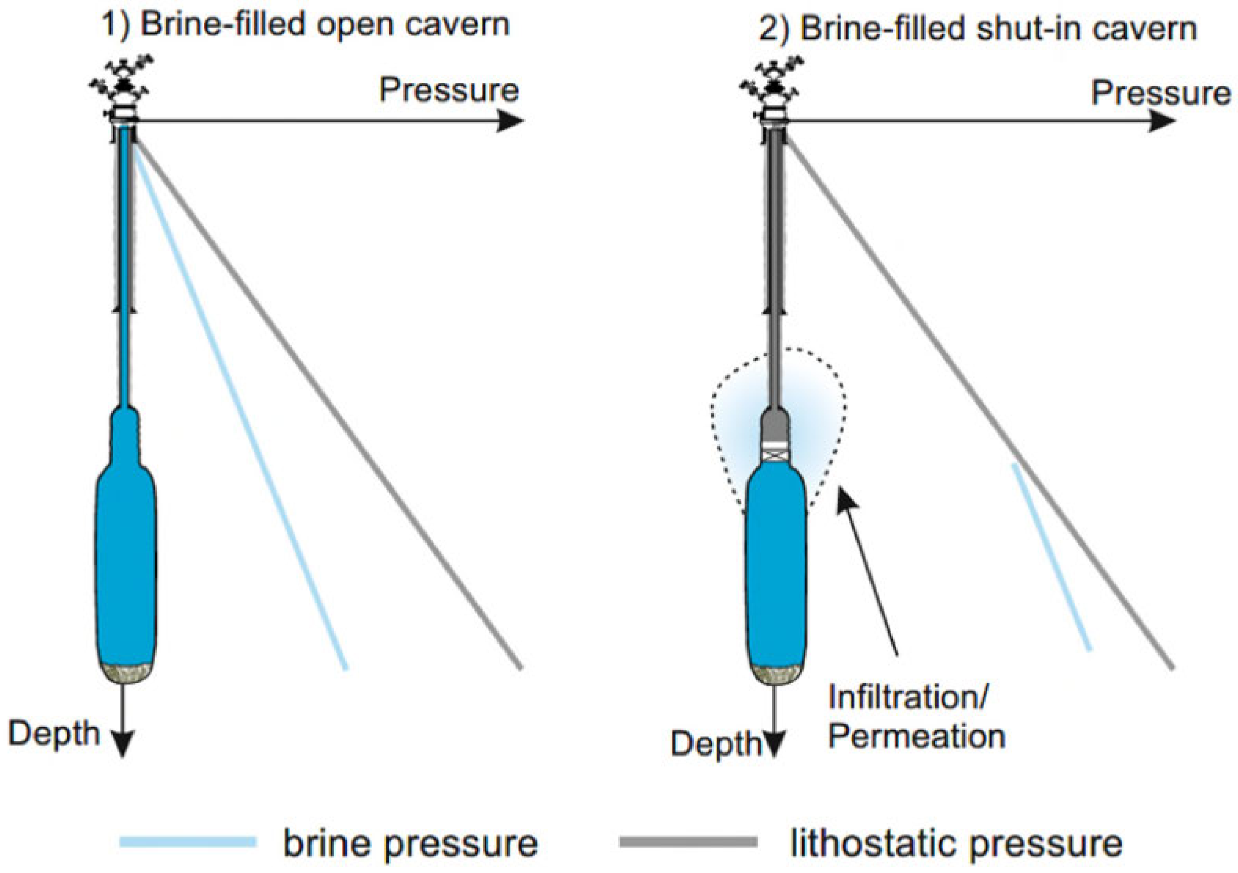

Figure 4-1: **Schematic illustration of the expected pressure development in a sealed cavern [BUZOGANY ET AL . 2022]**

For the purpose of convergence calculations, the cavern pressure at the cavern roof is considered with a gradient of 0.21 bar/m. The representative cavern pressure in the volumetric centre as applied for convergence calculations was then derived utilizing the halmostatic pressure gradient down from the cavern pressure in the cavern roof.

Thus, a constant convergence rate is assumed for the abandonment via hard shut-in.

It has to be noted that the influence of brine migration on surface subsidence is still not completely clarified. Fluid migration into the salt body generally means no or just a neglectable volume loss in the subsurface, since the compressibility of brine is limited. The migration of brine into the salt body rather results in the spatial redistribution of brine volume and therefore, the volume loss in open cavern volume compensated by volume gain in the infiltration/percolation zone at a different location. Therefore, as long as the brine migration takes place in the salt dome body, the effects of cavern convergence on surface subsidence during the hard shut-in phase can be considered as negligible even if field data confirming this process are limited. In case, the brine migration zone might reach the salt dome boundaries, depending on the local geology, the tightness of the caprock and the migration mechanisms outside of the salt body, the spatial redistribution of brine volume might reach wider distances and might result in a local “effective” volume loss in the investigation area. However, these processes and their influences on surface subsidence are currently still under investigation.

Therefore, in the context of the subsidence model it is conservatively assumed for the subsidence prediction that the total convergence volume generated during the hard shut-in will be transmitted to the surface.

4.2 Abandonment Scenario: Soft Shut-In

The second abandonment scenario investigated was the soft shut-in of the caverns. In this scenario, the caverns are initially shut-in when the standstill period begins. Comparable to the first scenario, the pressure inside the cavern will increase due to convergence of the cavern. However, when the maximum allowable pressure at the casing shoe is reached, the pressure is reduced by releasing brine.

No infiltration of brine into the overburden will occur, as the cavern pressure will respect the maximum pressure which ensures the geological tightness of the rock mass surrounding the cavern.

The maximum cavern pressure at the volumetric centre of the cavern can be derived from the maximum pressure at the LCCS (0.18 bar/m).

In the subsidence model, it is assumed that the cavern will always be depressurized by 10 bar after reaching the maximum pressure. Hence, it is assumed that the average cavern pressure during this scenario will be approx. 5 bar lower than the maximum cavern pressure.

List of References

[BEREST AND BROUARD, 1998] Bérest, P., & Brouard, B. (1998)
'A Tentative Classification of Salts According to their Creep Properties'. New Orleans: SMRI Spring Meeting.

[BEREST ET AL, 2008] Bérest, P., Brouard, B. & Karimi-Jafari (2008)
'THE EFFECT OF SMALL DEVIATORIC STRESS ON CAVERN BEHAVIOR'. Galveston: SMRI Fall Meeting.

[BUZOGANY 2019] Buzogany, R. (2019):
‚Erweiterung und Validierung eines Modells für die Prognose von Bodensenkungen infolge des Betriebs von Salzkavernen', Masterarbeit, Lehrstuhl für Bodenmechanik, Grundbau und Umweltgeotechnik', Bochum, 2019.

[BUZOGANY ET AL, 2022] Buzogany, R., Réveillère, A., Lampe, B. Borglum, S., Karimi-Jafari, M., Bernhardt, H. (2019):
‚Abandonment of Salt Caverns Phase 1: Gap Analysis', SMRI Research Report RR2022-1.

[DŻEGNIUK, NIEDOJADŁO & SROKA 2003] Dżegniuk, B., Niedojadło, Z., & Sroka, A. (2003)
‚Podstawy wymiarowania i eksploatacji szybowych filarów ochronnych'. Szkoła Eksploatacji Podziemnej.

[ECOLE POLYTECHNIQUE ET AL. 2020] Ecole Polytechnique; Brouard Consulting; Institut für Gebirgsmechanik; RESPEC; Storengy; Urai, Janos; Spiers, CJ; Peach, CJ (2020):
'Very Slow Creep Tests As a Basis for Cavern Stability Analysis, Phase 2'. SMRI Report RR2020-1.

[EIKEMEIER & HEUSERMANN, 2007] Eickemeier, R., Heusermann, S. (2007):
'Kavernenfelder Winschoten / Heiligerlee und Heiligerlee Senkungsprog- nosen für die Kavernenfelder Winschoten / Heiligerlee und Heiligerlee (Datenbasis 2005)'. Abschlussbericht – Anlagenband, Bundesanstalt für Geowissenschfaten und Rohstoffe (BGR), Hannover.

[FOKKER 2018] Fokker, P. A., Van Leijen, F. J., Orlic, B., Van Der Marel, H., & Hanssen, R. F. (2018).
'Subsidence in the Dutch Wadden Sea'. Netherlands Journal of Geosciences, 97(3), 129-181.

[GÜNTHER ET AL 2016] Günther, R. M., Lüdeling, C., Popp, T., Naumann, D., Wiedemann, M., & & Weise, D. (2016).
‚Vergleich aktueller Stoffgesetze und Vorgehensweisen anhand von Modellberechnungen zum thermo-mechanischen Verhalten und zur Verheilung von Steinsalz - Teilvorhaben, 2'.

[HENGST 2014] Hengst, G. (2014).
'Monitoring der durch Kavernenkonvergenz induzierten Bodensenkungen unter Betrachtung ihrer Wirkungen auf die ökologischen Zusammenhänge'. 15. Geokinematischer Tag, 15./16. May 2014. Freiberg, 237-251.

[KOOI ET AL 1998] Kooi, H., Johnston, P., Lambeck, K., Smither, C. & Molendijk, R. (1998)
'Geological causes of recent (~100 yr) vertical land movement in the Netherlands'. Tectonophysics 299: 297–316.

[PÖTTGENS, 1973] Pöttgens, J.J.E. (1973)
‚Bodemdaling zoitwinning concessive "Adolf van Nassau". (Vertrouwelijk rapport) Heerlen, 14 februari 1973, Staatstoezicht op de Mijnen

[QUASNITZA 1988] Quasnitza, H. (1988).
‚Eine Strategie zur Kalibrierung markschneiderischer Bewegungsmodelle und zur

Prädikation von Bewegungselementen‘ PhD thesis, Technische Universität Clausthal.

[SCHOBER ET AL. 1987] Schober, F., Sroka, A., Hartmann, A. (1987): ‘Ein Konzept zur Senkungsberechnung über Kavernenfeldern‘, Kali und Steinsalz, Bd. 9, Heft 11, 1987.

[SROKA & SCHOBER 1982] Sroka, A., Schober, F. (1982): ‘Die Berechnung der maximalen Bodenbewegung über kavernenartigen Hohlräumen unter Berücksichtigung der Hohlraumgeometrie‘, Kali und Steinsalz, 1982.

[SROKA ET AL. 1987] Sroka A., Schober F., & Sroka T. (1987). ‘Ogólne zależności między wybraną objętością pustki poeksploatacyjnej a objętością niecki osiadania z uwzględnieniem funkcji’ Ochrona Terenów Górniczych, 79/1, Katowice.

[SROKA ET AL. 2017] Sroka, A., Misa, R., Tajdus, K., Klaus, M., Meyer, S., & Feldhaus, B. (2017). ‘Forecast of rock mass and ground surface movements caused by the convergence of salt caverns for storage of liquid and gaseous energy carriers’ Freiberg: 18. Geokinematischer Tag.

[URAI, SCHMATZ & KLAVER 2019] Urai, J., Schmatz, J., & Klaver, J. (2019): ‘Over-pressured salt solution mining caverns and leakage mechanisms; Phase 1: micro-scale processes’, Project KEM-17.

[URAI & SPIERS 2007] Urai, J., & Spiers, C. (2007). ‚The effect of grain boundary water on deformation mechanisms and rheology’ The Mechanical Behavior of Salt - 6th Conference (SaltMech6), Hannover.

[WEP 2010] Well Engineering Partners B.V. Hoogeveen (2010) ‘FRISIA cavern abandonment – BAS-3’

[WEP 2015] Well Engineering Partners B.V. Hoogeveen (2015) ‘Abandonment study Nedmag caverns - Cavern squeeze modeling and geophysical analysis of brine permeation and containment’

[VAN SAMBEEK & DIRIENZO 2016] Van Sambeek, L., DiRienzo, A. (2016) ‘Analytical Solutions for Stress Distributions and Creep Closure Around Open-Holes or Caverns Using Multilinear Segmented Creep Laws’, Salzburg: SMRI Fall Meeting

[ZANDER 2007] Zander-Schiebenhöfer, D. (2007): ‘Kriechverhalten von Salzgestein in der Umgebung von Kavernenfeldern‘, Dissertation, Fakultät für Bauingenieurwesen und Geodäsie, Gottfried Wilhelm Leibniz Universität, Hannover, 2007.